

All-oxide spin Seebeck effects

Z. Qiu^{*,1,2} D. Hou^{1,2} K. Uchida^{2,3,4} and E. Saitoh^{1,2,3,5}

¹*WPI Advanced Institute for Materials Research,*

Tohoku University, Sendai 980-8577, Japan

²*Spin Quantum Rectification Project, ERATO,*

Japan Science and Technology Agency, Sendai 980-8577, Japan

³*Institute for Materials Research, Tohoku University, Sendai 980-8577, Japan*

⁴*PRESTO, Japan Science and Technology Agency, Saitama 332-0012, Japan*

⁵*Advanced Science Research Center,*

Japan Atomic Energy Agency, Tokai 319-1195, Japan

Abstract

We report the observation of longitudinal spin Seebeck effects (LSSE) in an all-oxide bilayer system comprising an IrO_2 film and an $\text{Y}_3\text{Fe}_5\text{O}_{12}$ film. Spin currents generated by a temperature gradient across the $\text{IrO}_2/\text{Y}_3\text{Fe}_5\text{O}_{12}$ interface were detected as electric voltage via the inverse spin Hall effect in the conductive IrO_2 layer. This electric voltage is proportional to the magnitude of the temperature gradient and its magnetic field dependence is well consistent with the characteristic of the LSSE. This demonstration may lead to the realization of low-cost, stable, and transparent spin-current-driven thermoelectric devices.

* Author to whom correspondence should be addressed; electronic mail: qiuzy@imr.tohoku.ac.jp

The spin Seebeck effect (SSE) generates spin voltage in a magnetic material as a result of a temperature gradient [1–19]. Since the thermally generated spin voltage induces a spin current across the interface between the magnetic material and an adjacent conductive material, it can be detected as electric voltage via the inverse spin Hall effect (ISHE) in the conductive layer. Therefore, a magnetic/conductive bilayer system is commonly used for the SSE study [7–19]. The SSE has attracted increasing attention because of the possible applications for thermoelectric conversion and spintronic devices [16, 20], and investigation of the SSE in various materials is important to further improvement of thermoelectric and thermo-spin conversion efficiency. However, all the experimental studies on the SSE to date have been performed using simple metals as conductive layers, while wide variety of materials have been investigated for the magnetic layer [7, 8, 19].

As alternate conductive materials for the SSE devices, conductive oxides can be good candidates because of the low cost, good chemical stability, and easy preparation of oxides. In addition, conductive oxide films can often be transparent. Therefore, the conductive oxides enable the construction of transparent thermoelectric and thermo-spin devices, making it more suitable for applications requiring transparency, such as applications to smart windows.

In this work, we report the observation of the SSE in an all-oxide bilayer system comprising a conductive IrO_2 and a ferrimagnetic insulator $\text{Y}_3\text{Fe}_5\text{O}_{12}$ (YIG). Here, YIG is one of most widely used materials for spin-current studies since it has a small Gilbert damping constant, long spin-wave-propagation length, and high electrical resistivity [9–17, 21–23]. We select IrO_2 for detecting the SSE since relatively-high spin-Hall angle has been reported in this conductive oxide [24–26]. Importantly, IrO_2 is an n-type transparent semiconductor of which its work function is very close to metals, such as Ag [27], making it easier to form an Ohmic contact between IrO_2 and metallic electrodes [26]. This situation is indispensable for detecting the ISHE in IrO_2 if the output voltage is in the order of submicrovolts or less.

To investigate the SSE in the all-oxide system, a longitudinal configuration is employed in this work [10, 11]. In Fig. 1(a), we show a schematic illustration of the experimental configuration and the sample structure of the IrO_2 /YIG bilayer film for measuring the longitudinal SSE (LSSE). The single-crystalline YIG film was grown on a 0.5-mm-thick (111) $\text{Gd}_3\text{Ga}_5\text{O}_{12}$ (GGG) substrate by using a liquid phase epitaxy method. The thickness of the YIG film is about 4.5 μm . A 30-nm-thick IrO_2 film was then deposited on the YIG film by using an rf-sputtering method at room temperature. As shown in Fig. 1(b), the

light transmittance of the 30-nm-thick IrO₂ film is much higher than that of a conventional 10-nm-thick Pt film in the visible light range.

The LSSE measurements were performed by using an experimental setup similar to that described in Ref. [11]. The IrO₂/YIG sample with the size of $2 \times 6 \text{ mm}^2$ was sandwiched between two AlN heat baths of which the temperatures were stabilized to $300 \text{ K} + \Delta T$ and 300 K , where the temperature of the heat bath connected to the top of the IrO₂ layer is higher than that connected to the bottom of the GGG substrate. The temperature difference ΔT was generated by using a Peltier thermoelectric module and detected by using thermocouples.

The temperature gradient across the IrO₂/YIG interface induces a spin current in the IrO₂ layer along the direction normal to the interface if the magnetic moments in YIG and conduction-carriers' spins in IrO₂ are coupled via the spin-mixing conductance. This spin current is converted into an electric field \mathbf{E}_{ISHE} by the ISHE in the IrO₂ layer along the direction determined by the following relation:

$$\mathbf{E}_{\text{ISHE}} = g_{\text{r}}^{\uparrow\downarrow} \frac{\theta_{\text{SHE}} \lambda \rho}{d} \mathbf{j}_{\text{s}} \times \frac{\mathbf{M}}{|\mathbf{M}|}, \quad (1)$$

where \mathbf{j}_{s} , θ_{SHE} , ρ , λ , and d denote the spatial direction of the thermally generated spin current, spin-Hall angle, resistivity, spin-diffusion length, and thickness of the IrO₂ film, respectively. $g_{\text{r}}^{\uparrow\downarrow}$ is the real part of the spin-mixing conductance at the IrO₂/YIG interface and \mathbf{M} is the magnetization vector of the YIG film. In Eq. (1), we neglect the diffusion term of the spin current in the IrO₂ film because d ($= 30 \text{ nm}$) of our sample is much greater than λ of IrO₂ ($= 3.8 \text{ nm}$ [26]). The LSSE-induced \mathbf{E}_{ISHE} in the IrO₂ layer can be detected as an electric voltage signal $V_{\text{ISHE}} = E_{\text{ISHE}} l$ with E_{ISHE} and l respectively being the magnitude of \mathbf{E}_{ISHE} and the effective sample length. To measure V_{ISHE} induced by the LSSE in the IrO₂/YIG sample, two silver-paste electrodes were attached to the ends of the IrO₂ layer with the interval of $l = 4 \text{ mm}$ and the electric voltage difference V between the two electrodes was measured with sweeping an external magnetic field H at various values of ΔT .

Figure 2(b) shows the H dependence of V for various values of ΔT for the IrO₂/YIG sample, measured when the magnetic field was applied along the y direction. As ΔT increases, a clear voltage signal was found to appear in the IrO₂ layer in response to the magnetization reversal of the YIG layer, while no signal was observed at $\Delta T = 0 \text{ K}$. The voltage signal is

proportional to ΔT , and its linear fitting line shows that the thermopower in the IrO₂/YIG sample is $V/\Delta T = 0.021 \mu\text{VK}^{-1}$ [see Fig. 2(c)]. These results indicate that the voltage signal is attributed to the ISHE in the IrO₂ layer generated by the LSSE in the YIG layer.

To further confirm the origin of the thermoelectric voltage in the IrO₂/YIG sample, we measured V with changing the angle of the external magnetic field. Figure 3 shows the H dependence of V for the IrO₂/YIG sample at $\Delta T = 9$ K for various values of the out-of-plane field angle θ_H , where θ_H is defined as in the upper left panel of Fig. 3. When $\theta_H \neq 0^\circ$, finite V signals appear and their magnitude and sign systematically change with θ_H . In contrast, no V signal was observed when the magnetic field is perpendicular to the film surface: $\theta_H = 0^\circ$. The θ_H dependence of V in the IrO₂/YIG sample is well reproduced by Eq. (1) combined with static demagnetizing fields in the YIG film (see Fig. 4), consistent with the symmetry of the ISHE voltage induced by the LSSE.

In Fig. 5, we show the comparison of the LSSE signals between the IrO₂/YIG sample and conventional Pt/YIG sample. The Pt/YIG sample was prepared by sputtering a 10-nm-thick Pt film on YIG/GGG wafer, where the YIG films for the IrO₂/YIG and Pt/YIG samples were grown at the same time. Both the samples have the same size ($2 \times 6 \text{ mm}^2$) and the LSSE measurements were carried out in the same condition at $\Delta T = 9$ K. The magnitude of the LSSE signal in the IrO₂/YIG sample was found to be 68 times smaller than that in the Pt/YIG sample. Such a small LSSE signal in the IrO₂/YIG sample is attributed not only to the thicker thickness of the IrO₂ layer but also to the small spin-mixing conductance at the IrO₂/YIG interface; by using Eq. (1) with $\theta_{\text{SHE}} \cdot \lambda = 0.152 \text{ nm}$ [26] (0.188 nm [28]) and $\rho = 2.7 \times 10^{-4} \Omega\text{cm}$ ($4.5 \times 10^{-5} \Omega\text{cm}$) for the IrO₂ (Pt) film and $g_{\text{r}}^{\uparrow\downarrow} = 1.3 \times 10^{18} \text{ m}^{-2}$ at the Pt/YIG interface [29], the spin mixing conductance at the IrO₂/YIG interface is estimated to be $g_{\text{r}}^{\uparrow\downarrow} = 1.2 \times 10^{16} \text{ m}^{-2}$. Therefore, improvement of the spin-mixing conductance at the conductive-oxide/magnetic-insulator interface is indispensable to realizing efficient all-oxide SSE devices, which may be achieved, for example, by improving crystalline structure of the interface by annealing treatment[29], by modulating carrier density in the conductive oxide layer, and by inserting magnetic interlayers between the conductive-oxide and magnetic-insulator layers[30].

In summary, we measured the longitudinal spin-Seebeck effect (LSSE) in the all-oxide IrO₂/Y₃Fe₅O₁₂ (YIG) bilayer film. The temperature-difference, magnetic-field, and field-angle dependences of the thermoelectric voltage in the IrO₂/YIG sample are well consistent

with the characteristics of the inverse spin-Hall effect in the IrO_2 layer induced by the LSSE in the YIG layer. The LSSE voltage in the IrO_2/YIG sample was observed to be much smaller than that in a conventional Pt/YIG sample, which may be attributed to the small spin-mixing conductance at the IrO_2/YIG interface if the spin-Hall angle and spin-diffusion length of our IrO_2 film are assumed to be comparable to those reported by previous studies. Although an all-oxide system is one of promising candidates for realizing low-cost, stable, and transparent LSSE thermospin devices, major improvement of the spin-mixing conductance at conductive-oxide/magnetic-insulator interfaces is necessary.

The authors thank A. Kirihara and M. Ishida for valuable discussions. This work was supported by PRESTO “Phase Interfaces for Highly Efficient Energy Utilization”, Strategic International Cooperative Program ASPIMATT from JST, Japan, Grant-in-Aid for Young Scientists (A) (25707029), Grant-in-Aid for Challenging Exploratory Research (26600067), Grant-in-Aid for Scientific Research (A) (24244051), Grant-in-Aid for Scientific Research on Innovative Areas “Nano Spin Conversion Science” (26103005) from MEXT, Japan, and NEC Corporation.

-
- [1] M. Weiler, M. Althammer, F. D. Czeschka, H. Huebl, M. S. Wagner, M. Opel, I. M. Imort, G. Reiss, A. Thomas, R. Gross, et al., *Physical Review Letters* **108**, 106602 (2012).
 - [2] K. Uchida, S. Takahashi, K. Harii, J. Ieda, W. Koshibae, K. Ando, S. Maekawa, and E. Saitoh, *Nature* **455**, 778 (2008).
 - [3] C. M. Jaworski, J. Yang, S. Mack, D. D. Awschalom, J. P. Heremans, and R. C. Myers, *Nature Materials* **9**, 898 (2010).
 - [4] D. Qu, S. Y. Huang, J. Hu, R. Wu, and C. L. Chien, *Physical Review Letters* **110**, 067206 (2013).
 - [5] M. Agrawal, V. I. Vasyuchka, A. A. Serga, A. Kirihara, P. Pirro, T. Langner, M. B. Jungfleisch, a. V. Chumak, E. T. Papaioannou, and B. Hillebrands, *Physical Review B* **89**, 224414 (2014).
 - [6] S. M. Rezende, R. L. Rodríguez-Suárez, R. O. Cunha, A. R. Rodrigues, F. L. A. Machado, G. A. Fonseca Guerra, J. C. Lopez Ortiz, and A. Azevedo, *Physical Review B* **89**, 014416 (2014).
 - [7] R. Ramos, T. Kikkawa, K. Uchida, H. Adachi, I. Lucas, M. H. Aguirre, P. Algarabel, L. M.

- On, S. Maekawa, E. Saitoh, and M. R. Ibarra, *Appl. Phys. Lett.* **102**, 072413 (2013).
- [8] D. Meier, T. Kuschel, L. Shen, A. Gupta, T. Kikkawa, K. Uchida, E. Saitoh, J. M. Schmalhorst, and G. Reiss, *Physical Review B* **87**, 054421 (2013).
- [9] K. Uchida, J. Xiao, H. Adachi, J. Ohe, S. Takahashi, J. Ieda, T. Ota, Y. Kajiwara, H. Umezawa, H. Kawai, G. E. W. Bauer, S. Maekawa, and E. Saitoh, *Nature Materials* **9**, 894 (2010).
- [10] K. Uchida, H. Adachi, T. Ota, H. Nakayama, S. Maekawa, and E. Saitoh, *Applied Physics Letters* **97**, 172505 (2010).
- [11] K. Uchida, T. Ota, H. Adachi, J. Xiao, T. Nonaka, Y. Kajiwara, G. E. W. Bauer, S. Maekawa, and E. Saitoh, *Journal of Applied Physics* **111**, 103903 (2012).
- [12] T. Kikkawa, K. Uchida, S. Daimon, Y. Shiomi, H. Adachi, Z. Qiu, D. Hou, X. F. Jin, S. Maekawa, and E. Saitoh, *Physical Review B* **88**, 214403 (2013).
- [13] T. Kikkawa, K. Uchida, Y. Shiomi, Z. Qiu, D. Hou, D. Tian, H. Nakayama, X. F. Jin, and E. Saitoh, *Physical Review Letters* **110**, 067207 (2013).
- [14] A. Kirihara, K. Uchida, Y. Kajiwara, M. Ishida, Y. Nakamura, T. Manako, E. Saitoh, and S. Yorozu, *Nature Materials* **11**, 686 (2012).
- [15] N. Roschewsky, M. Schreier, A. Kamra, F. Schade, K. Ganzhorn, S. Meyer, H. Huebl, R. Gross, and S. T. B. Goennenwein, *Applied Physics Letters* **104**, 202410 (2014).
- [16] K. Uchida, M. Ishida, T. Kikkawa, A. Kirihara, T. Murakami, and E. Saitoh, *Journal of Physics: Condensed matter* **26**, 343202 (2014).
- [17] K. Uchida, T. Kikkawa, A. Miura, J. Shiomi, and E. Saitoh, *Phys. Rev. X* **4**, 041023 (2014).
- [18] M. Schreier, N. Roschewsky, E. Dobler, S. Meyer, H. Huebl, R. Gross, and S. T. B. Goennenwein, *Applied Physics Letters* **103**, 242404 (2013).
- [19] K. Uchida, T. Nonaka, T. Kikkawa, Y. Kajiwara, and E. Saitoh, *Physical Review B* **87**, 104412 (2013).
- [20] G. E. W. Bauer, E. Saitoh, and B. J. van Wees, *Nature Materials* **11**, 391 (2012).
- [21] S. Geller and M. A. Gilleo, *Acta Crystallographica* **10**, 239 (1957).
- [22] V. Cherepanov, I. Kolokolov, and V. L'vov, *Physics Reports* **229**, 81 (1993).
- [23] A. A. Serga, A. V. Chumak, and B. Hillebrands, *Journal of Physics D-Applied Physics* **43**, 264002 (2010).
- [24] Z. Qiu, T. An, K. Uchida, D. Hou, Y. Shiomi, Y. Fujikawa, and E. Saitoh, *Applied Physics*

- Letters **103**, 182404 (2013).
- [25] Z. Qiu, Y. Kajiwara, K. Ando, Y. Fujikawa, K. Uchida, T. Tashiro, K. Harii, T. Yoshino, and E. Saitoh, Applied Physics Letters **100**, 022402 (2012).
 - [26] K. Fujiwara, Y. Fukuma, J. Matsuno, H. Idzuchi, Y. Niimi, Y. Otani, and H. Takagi, Nature Communications **4**, 2893 (2013).
 - [27] B. R. Chalamala, Y. Wei, R. H. Reuss, S. Aggarwal, B. E. Gnade, R. Ramesh, J. M. Bernhard, E. D. Sosa, and D. E. Golden, Applied Physics Letters **74**, 1394 (1999).
 - [28] J. C. Rojas-Sánchez, N. Reyren, P. Laczkowski, W. Savero, J. P. Attané, C. Deranlot, M. Jamet, J. M. George, L. Vila, and H. Jaffrès, Physical Review Letters **112**, 106602 (2014).
 - [29] Z. Qiu, K. Ando, K. Uchida, Y. Kajiwara, R. Takahashi, H. Nakayama, T. An, Y. Fujikawa, and E. Saitoh, Applied Physics Letters **103**, 092404 (2013).
 - [30] D. Kikuchi, M. Ishida, K. Uchida, Z. Qiu, T. Murakami, and E. Saitoh, Appl. Phys. Lett. **106**, 082401 (2015).

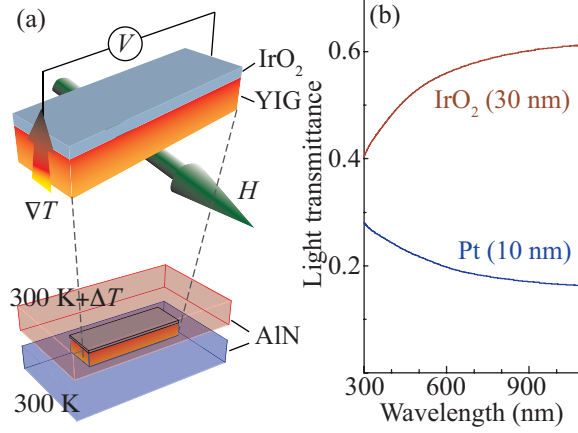


FIG. 1: (a) A schematic illustration of the IrO₂/YIG sample and experimental configuration for measuring the LSSE. ∇T and H denote the temperature gradient and the external magnetic field, respectively. The sample was sandwiched between two AlN heat baths, of which the temperatures were stabilized to 300 K + ΔT and 300 K, respectively. (b) Comparison of light transmittance spectra of a 30-nm-thick IrO₂ film and a 10-nm-thick Pt film. The films were formed on glass substrates, and the contribution from the light transmittance of the substrates is subtracted.

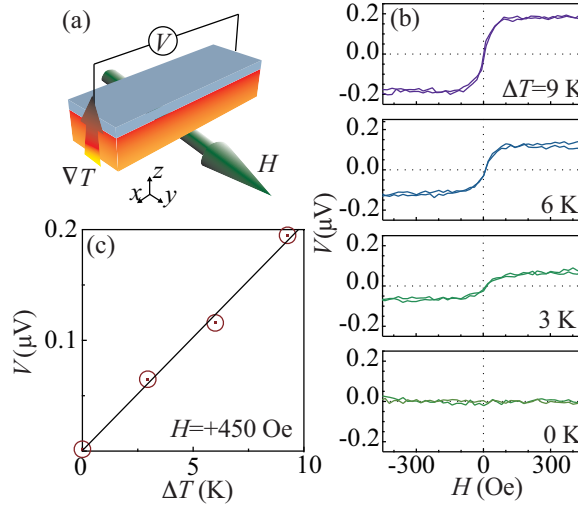


FIG. 2: (a) A schematic illustration of the IrO₂/YIG sample. (b) H dependence of the electric voltage V in the IrO₂/YIG sample for various values of ΔT . (c) ΔT dependence of V at $H = +450$ Oe in the IrO₂/YIG sample, measured when ∇T was applied along the $+z$ direction.

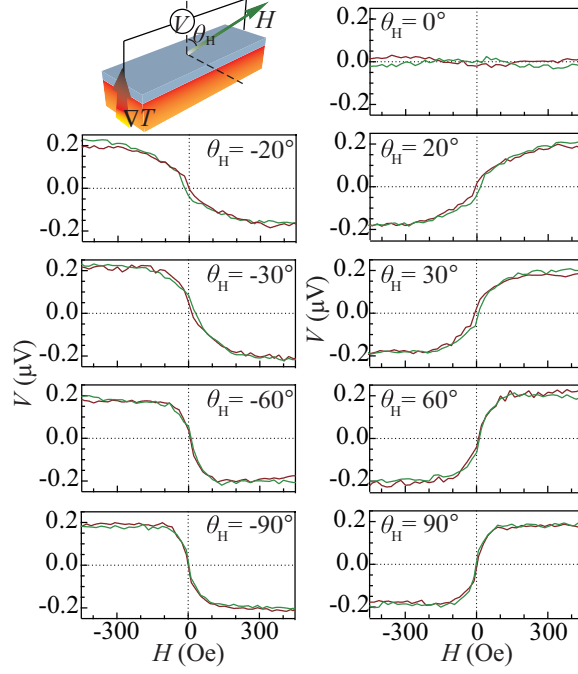


FIG. 3: H dependence of V in the IrO_2/YIG sample at $\Delta T = 9$ K for various values of the out-of-plane field angle θ_H .

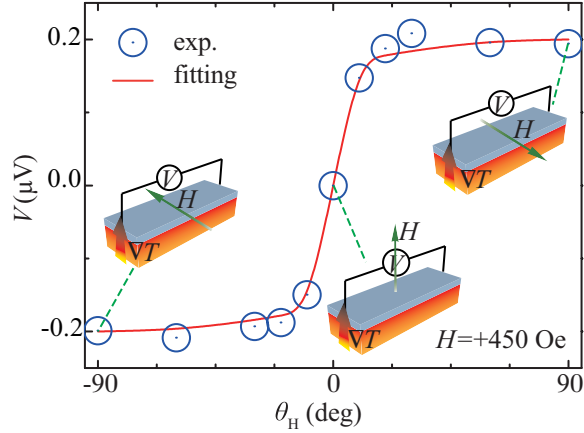


FIG. 4: θ_H dependence of V in the IrO_2/YIG sample at $H = +450$ Oe. The solid line was obtained by fitting the experimental data with Eq. (1) combined with static demagnetizing fields in the YIG film.

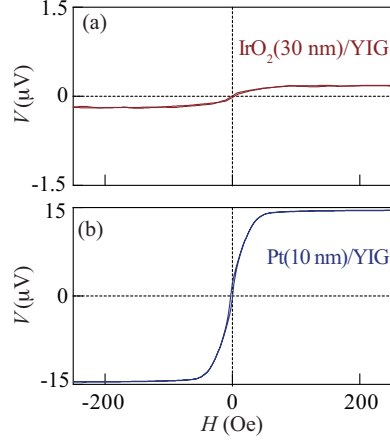


FIG. 5: H dependence of V in the IrO_2/YIG (a) and Pt/YIG (b) samples at $\Delta T = 9 \text{ K}$. The thickness of the IrO_2 (Pt) layer of the IrO_2/YIG (Pt/YIG) sample is 30 nm (10 nm).